



OPEN

Stochastic dynamics of a few sodium atoms in presence of a cold potassium cloud

Rohit Prasad Bhatt[✉], Jan Kilinc, Lilo Höcker & Fred Jendrzejewski[✉]

Single particle resolution is a requirement for numerous experimental protocols that emulate the dynamics of small systems in a bath. Here, we accurately resolve through atom counting the stochastic dynamics of a few sodium atoms in presence of a cold potassium cloud. This capability enables us to rule out the effect of inter-species interaction on sodium atom number dynamics, at very low atomic densities present in these experiments. We study the noise sources for sodium and potassium in a common framework. Thereby, we assign the detection limits to 4.3 atoms for potassium and 0.2 atoms (corresponding to 96% fidelity) for sodium. This opens possibilities for future experiments with a few atoms immersed in a quantum degenerate gas.

The random evolution of a small system in a large bath can only be described by its statistical properties. Such stochastic dynamics occur in a wide range of settings including financial markets¹, biological systems², impurity physics³ and quantum heat engines⁴. Their evolution is hard to predict from microscopic principles, stimulating strong efforts to realize highly controlled model systems in optomechanics⁵, cavity QED⁶, superconducting circuits⁷, trapped ions⁸ and cold atoms⁹. The evolution of the small system can be precisely accessed experimentally through various quantum information protocols like state tomography^{10,11}, random unitaries^{12,13} or out-of-time-order correlations¹⁴. However, for a bath with many degrees of freedom these protocols can become very resource intensive. Statistical approaches like the precise analysis of higher-order correlation functions of a many-body system^{14–16} or the extraction of entanglement through fluctuations^{17,18} offer an efficient alternative in this regime.

Cold atomic mixtures offer a natural mapping of physical phenomena involving system and bath, wherein one species realizes the bath, while the other species represents the system. If a mesoscopic cloud of the first species is immersed in a Bose–Einstein condensate formed by the second species, it implements the Bose polaron problem^{19–22}. In recent quantum simulators of lattice gauge theories, the small clouds of one species emulate the matter field, while the gauge field is realized by the second atomic species^{23–25}. The feasibility of immersing a few atoms into a large cloud was demonstrated in a dual-species magneto-optical trap (MOT) of rubidium and cesium²⁶. This was extended towards the study of position- and spin-resolved dynamics of a single tracer atom acting as a probe^{27,28}. These microscopic degrees of freedom remain inaccessible for the large cloud with macroscopic number of atoms⁴. While the study of the many-body systems will involve the controlled immersion of single atoms in a tweezer into a BEC, it is already possible to benchmark the properties of system and bath in simpler experimental setups.

Here, we focus on the stochastic dynamics of a few sodium atoms and a large cloud of potassium atoms in a dual-species MOT as shown in Fig. 1. In a MOT, cooling and trapping is achieved through a combination of magnetic field gradients with continuous absorption and emission of resonant laser light. We collect the resulting fluorescence on a dedicated camera for each species and trace their spatially integrated dynamics. This enables us to present a common statistical analysis for the dynamics of both species, which separates the fluctuations induced by the statistical loading process from those caused by technical limitations. Furthermore, we achieve single atom counting for sodium, which we employ to study its full counting statistics. This opens the possibility for future studies on the emergence of ergodicity and marks a first step towards position-resolution^{29,30} without a pinning lattice²⁷. Our work builds upon atom counting experiments with a single atomic species^{31–34} and atomic mixtures of Rb and Cs^{26, 35,36}. We extend the techniques towards a mixture of ²³Na and ³⁹K, which has shown excellent scattering properties in the degenerate regime³⁷. It therefore lays the ground work for experiments in the strongly correlated regimes, where single atoms are trapped in defect-free optical tweezer arrays^{38,39} and coupled to the bath in form of a large Bose–Einstein condensate.

Kirchhoff-Institut für Physik, Universität Heidelberg, Im Neuenheimer Feld 227, 69120 Heidelberg, Germany. ✉email: rohit.prasad@kip.uni-heidelberg.de; fnj@kip.uni-heidelberg.de

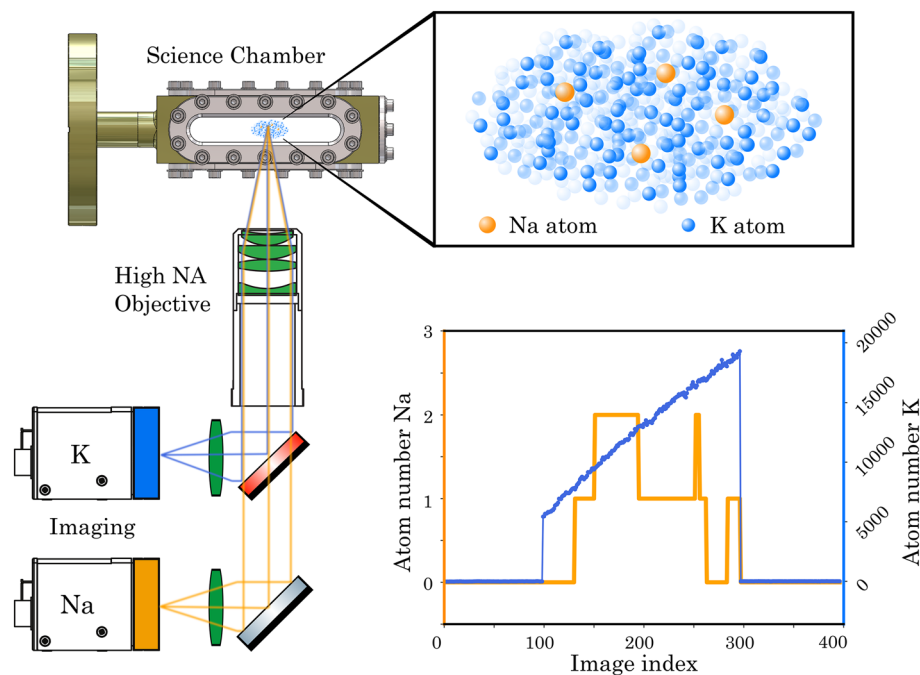


Figure 1. Experimental platform for atom counting. The atoms are trapped and laser cooled in a dual-species MOT inside the science chamber. The emitted fluorescence is collected by a high-resolution imaging system onto the cameras. We observe the stochastic dynamics of single sodium atoms (orange) surrounded by a large cloud of potassium atoms (blue).

The paper is structured as follows. In "[Experimental apparatus](#)" section, we provide a detailed discussion of the experimental apparatus, and how it is designed to fulfill the requirements of modern quantum simulators. In "[Atom number dynamics](#)" section, we study the dynamics of the observed fluorescence signal for both atomic species. The analysis of their mean and variance after an ensemble average is then employed to statistically investigate the origin of different fluctuations. In "[Full counting statistics of sodium](#)" section, we leverage the single atom counting resolution of sodium to extract the full counting statistics of atom load and loss events. In contrast to previous experiments with sodium and potassium^{37,40}, we operate at such low atomic densities that the presence of the potassium cloud has no measurable effect on the counting statistics of sodium. In "[Outlook](#)" section, we end with an outlook of the next steps for the experimental platform.

Experimental apparatus

In this section, we describe the different elements of our experimental apparatus. In the course of designing this machine, effort was taken to optimize the versatility and stability of the system. To achieve this, the experimental setup was designed for a continuous development of the vacuum and the laser system.

Vacuum system. Ultracold atom experiments require an ultra-high vacuum (UHV) at pressures below 10^{-11} mbar, in order to isolate the cold atoms from the surrounding environment. Common designs consist of a dual-species oven and a single Zeeman slower connected to a science chamber^{25,41–44}. In this design the first cooling stages of the two species are highly coupled, which renders the optimization of the system complex. In our vacuum system, we decoupled the precooling stages of sodium and potassium up to the science chamber, as sketched in Fig. 2. The compact vacuum system contains two independent two-dimensional magneto-optical trap (2D-MOT) chambers for sodium and potassium and a dual-species science chamber, where experiments are performed^{45,46}. The two 2D-MOT chambers are connected to the science chamber from the same side under a 12.5° angle. The entire apparatus is mounted on a $600\text{ mm} \times 700\text{ mm}$ aluminium breadboard, which is fixed to a linear translation stage, inspired by ref.³⁹. Therefore, we are able to move the science chamber out of the contraction of magnetic field coils and optics. This allows for independent improvement of the vacuum system and in-situ characterization of the magnetic field at the position of the atoms.

2D-MOT. The design of the 2D-MOT setup is inspired by ref.⁴⁶. The chamber body is manufactured from titanium (fabricated by SAES Getters), where optical access is ensured by standard CF40 fused silica viewports with broadband anti-reflection coating (BBR coating). The 2D-MOT region has an oven containing a 1 g atomic ingot ampoule. The oven is heated to 160°C (70°C) for sodium (potassium), thereby increasing the pressure to 10^{-8} mbar in this region. To maintain an UHV in the science chamber, a differential pumping stage separates the two vacuum regions from each other. Two gate valves ensure full decoupling of the two atomic species by isolating different chambers. Each region is pumped with its separate ion getter pump (*NEXTorr Z100* and *NEXTorr D500* from SAES Getters). We employed four stacks of nine (four) neodymium bar magnets to generate the required magnetic quadrupole field inside the sodium (potassium) 2D-MOT chamber.

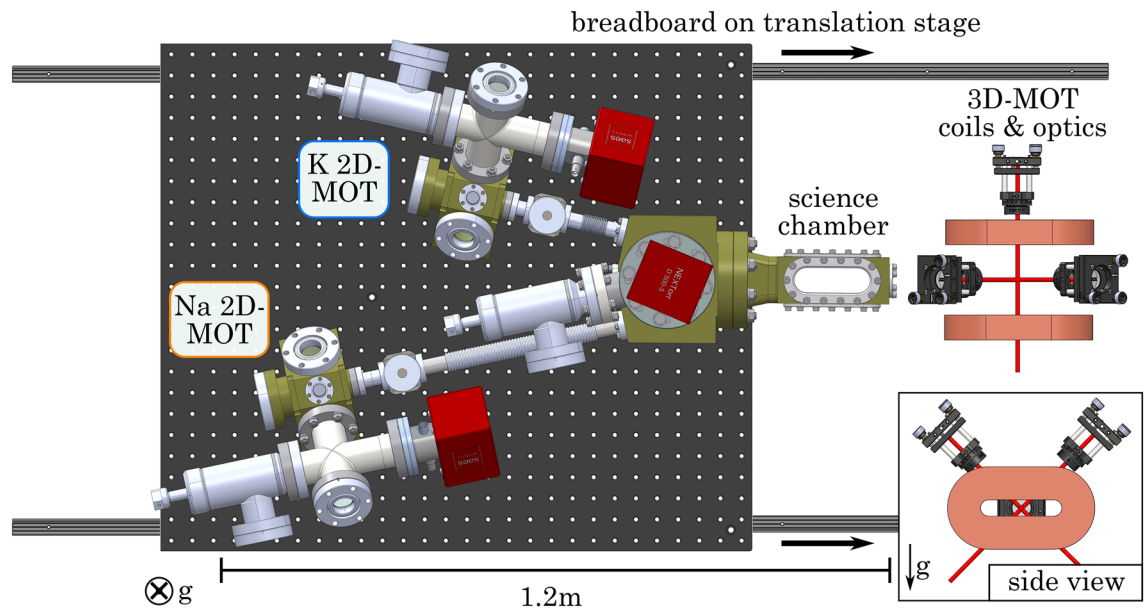


Figure 2. Vacuum system. The separated 2D-MOT chambers are connected from the same side to the dual-species science chamber. The vacuum pumps are shown in red. The whole vacuum system is mounted on a translation stage, such that the science chamber can be moved out of the region of the 3D-MOT coils and optics.

3D-MOT. The two atomic beams from the 2D-MOT chambers, coming in from the same side, have to intersect in the center of the science chamber. This constraint required us to use a custom rectangular titanium science chamber since for a glass chamber the glass-to-metal transition would require too much distance. Optical access for various laser beams and a high-resolution imaging system is maximized by four elongated oval viewports (fused silica, BBR coating), which are sealed using indium wire.

The quadrupole magnetic field required for the 3D-MOT is produced by the MOT coils, which are placed on the sides of the science chamber. Applying a current of 20 A to the coils results in a magnetic field gradient of 17 G/cm. The fast control of the current in the coils, required during an experimental sequence, is achieved through an insulated-gate bipolar transistor (IGBT) switching circuit. In order to cancel stray fields in the vicinity of the atomic clouds, we use three independent pairs of Helmholtz coils carrying small currents (< 1 A).

Laser cooling. In order to cool and trap the atoms, the laser light is amplified and frequency-stabilized on a dedicated optical table for each atomic species. The light is transferred to the main experiment table via optical fibers. The layout of the laser systems for both species is shown in Fig. 3.

Sodium. Laser cooling and trapping of sodium atoms is achieved using the D_2 -line at 589 nm, which is obtained from a high-power, frequency-doubled diode laser (*TA-SHG pro*, from *Toptica Photonics*). The laser light is stabilized to the excited-state crossover transition of the D_2 -line using saturated absorption spectroscopy (SAS) and Zeeman modulation locking⁴⁷. The modulated SAS signal is fed into a digital lock-in amplifier and PI-controller, which are programmed on a *STEMLab 125-14* board from *Red Pitaya* using the *Pyrrpl* module⁴⁸.

Potassium. Laser cooling and trapping of potassium atoms is achieved using the D_2 -line at 767 nm. The light is obtained from a master-slave laser configuration (both *DL pro*, from *Toptica Photonics*). The master laser frequency is locked to the ground-state crossover transition of the D_2 -line of ^{39}K with a scheme similar to sodium. The slave laser is frequency-stabilized through an offset beat lock (405 MHz) and its output is amplified to a power of 800 mW, using a home-built tapered amplifier module. This light is used to supply all the cooling and trapping beams. The offset locking scheme is designed to facilitate switching between the two isotopes, ^{39}K and ^{40}K . To cool the fermionic ^{40}K , the slave laser frequency should be increased by approximately 810 MHz via the offset lock, with the blue acousto-optic modulators (see Fig. 3) turned off and the electro-optic modulators turned on.

3D-MOT. On the experiment table, the light from the optical fibers is distributed into three independent paths for the operation of the dual-species MOT in a retro-reflected configuration. For both species the number of atoms loaded into the 3D-MOT can be tuned in a controlled way by adjusting the 2D-MOT beam power and the oven temperature. The 2D MOTs in our setup can produce an atomic flux of at least 10^8 atoms per second for sodium and at least 10^5 atoms per second for potassium. The pre-cooled atoms in the 2D-MOT region are transported to the 3D-MOT with a push beam. Such a setup has been used for the fast creation of Bose-Einstein condensates of sodium, as described in ref.^{46,49,50}.

For accurate atom counting of sodium, we use 1.3 mW power in each 3D-MOT beam and a beam diameter of about 2 mm, while the push and 2D-MOT beams are turned off. This helps in reducing the average loading rate to less than 3 atoms per minute as well as the stray light. Furthermore, the sodium oven is kept at a relatively low temperature of 80 °C (in contrast to the usual operating temperature of 160 °C for a bigger MOT), which increases the lifetime of atoms in the 3D-MOT due to better vacuum.

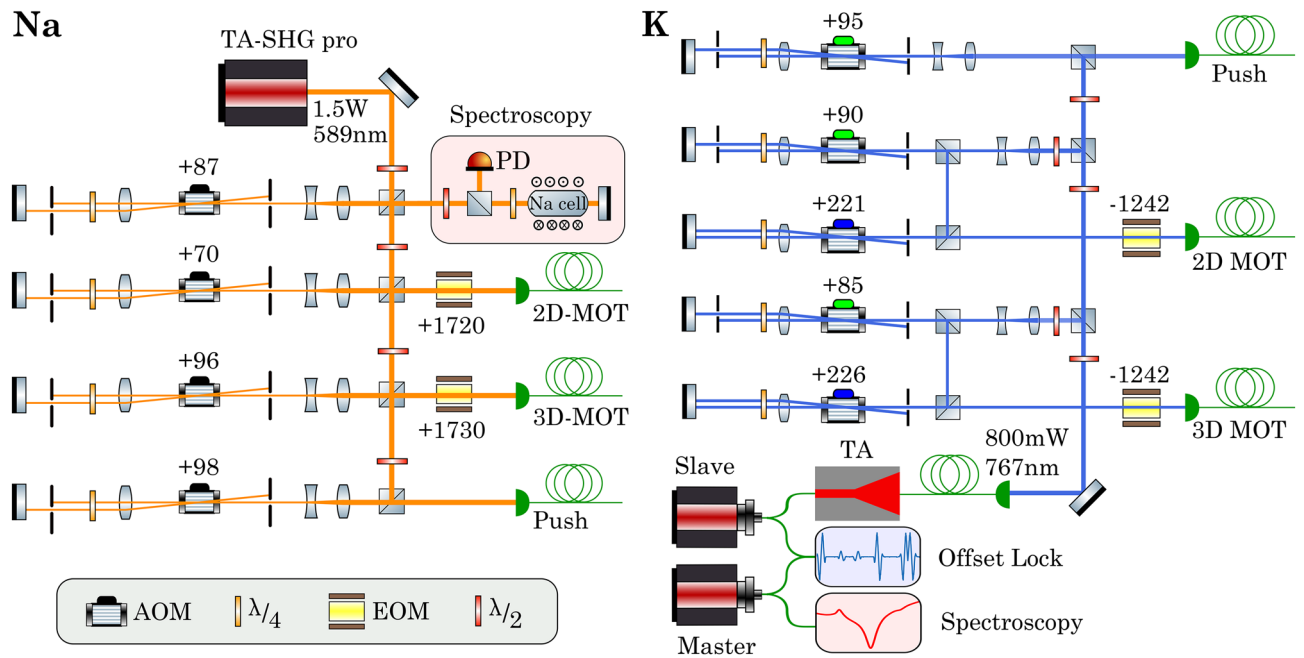


Figure 3. Sketch of the optical setup for laser cooling of sodium and potassium atoms. The laser light is split into different paths, enabling the individual control of laser power and frequency for the 2D-MOT, the 3D-MOT, and the push beam. The frequency and intensity of these beams is controlled with the help of acousto-optic modulators (AOMs) in double-pass configuration. The rf-frequencies for AOMs and EOMs are given in MHz. **Na:** The repumping light for the 2D- and 3D-MOT is generated by electro-optic modulators (EOMs). **K:** In the 2D- and 3D-MOT paths the green AOM controls the ^{39}K cooling frequency and the blue AOM is responsible for the creation of the ^{39}K repumping light. The repumping light for ^{40}K is generated by EOMs.

Fluorescence imaging. The cold atoms are characterized by collecting their fluorescence through an imaging system with a high numerical aperture (NA) onto a camera (Fig. 1). The imaging setup comprises an apochromatic high-resolution objective, which features an NA of 0.5 and chromatic focal correction in the wavelength range 589–767 nm (fabricated by *Special Optics*). The fluorescence of sodium and potassium is separated by a dichroic mirror, built into a cage system which is mounted on stages for x-, y- and z-translation along with tip-tilt adjustment.

Both imaging paths contain a secondary lens and an additional relay telescope (not displayed in Fig. 1 for clarity). This allows us to do spatial filtering with an iris in the intermediate image plane of the secondary lens and achieve a magnification of 0.75 (0.25) for sodium (potassium). For imaging the sodium atoms we use an sCMOS camera (*Andor Zyla 5.5*)^{51,52}, while for the potassium atoms we use an EMCCD camera (*NuVu HNu-512*). In total, we estimate the total conversion efficiency from photons to camera counts to be 0.2% (0.02%) for sodium (potassium).

Atom number dynamics

In this section, we describe the experiment for tracing the atom number dynamics of both species and study their evolution with a common statistical approach. Our experimental sequence is shown in Fig. 4A, where the timings are controlled with the *labcscript suite*⁵³. We start the atom dynamics by switching on the MOT magnetic field (with a gradient of 21 G/cm) and then monitor the fluorescence in $N_{\text{img}} = 200$ images. Each image has an integration time $\tau = 75$ ms, such that the camera counts overcome the background noise. Since the motion of the atoms during the integration time washes out any spatial information, we sum up the counts over the entire MOT region for each image. This results in a time trace of camera counts N_c , as shown in Fig. 4B. Each experimental run is preceded and succeeded by a series of 100 reference images to quantify the background noise Δ_{bg} , induced by the fluctuations in the stray light from the MOT beams.

The camera counts for sodium exhibit random jumps, corresponding to single atom load and loss events. The stochastic nature of the observed signal and large relative fluctuations require a statistical analysis of the dynamics in terms of expectation values. The single atom resolution provides additional access to the full counting statistics, which is discussed in "Full counting statistics of sodium" section. The few sodium atoms are surrounded by a cloud of potassium atoms, which we pre-load for 5s to ensure large atom numbers (up to $2 \cdot 10^4$ atoms). In contrast to sodium, we do not observe discrete jumps, but rather a continuous loading curve with higher counts and smaller relative fluctuations. These are typical features of a bath, which can be characterized by its mean and variance.

To extract expectation values through an ensemble average, we perform 100 repetitions of the previously described experimental sequence for sodium and potassium independently. Given the smaller size of the dataset, it was possible to increase the integration time τ , as the heating of the MOT coils was less of a limiting factor.

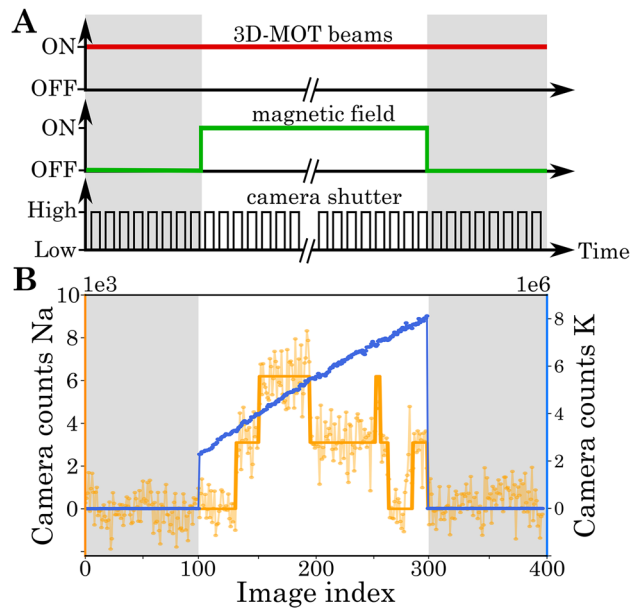


Figure 4. Experimental sequence. **A:** A series of images (black) is taken. While the MOT beams (red) are always on, the magnetic field (green) is switched off for reference images marked in grey. **B:** Typical time trace from the series of images of sodium (orange) and potassium (blue).

Therefore, we increased the integration time for sodium to 200 ms for the data shown in Figs. 5 and 6. To access a regime of reduced atom numbers (up to 60 atoms) of potassium in this analysis, we reduce the 2D-MOT power and do not perform pre-loading. The observed dynamics are shown in Fig. 5A. We calculate the mean \bar{N}_c and standard deviation Δ_c of counts at each image index^{54,55}. For the case of sodium, the dynamics is so slow that it never reaches a stationary regime during a time trace. Furthermore, the amplitude of the fluctuations is comparable to the average camera counts throughout the entire observation. For potassium, the stationary situation is achieved on average after a few seconds of loading. Once again, we observe a strong dependence of the standard deviation on the average atom counts.

To study this dependence quantitatively, we trace the variance Δ_c^2 as a function of the average counts \bar{N}_c in Fig. 5B. For sodium the variance shows a linear dependence on the average counts with an intercept. This behavior can be understood by considering two independent noise sources. The first one is a background noise Δ_{bg} , which is independent of the atom number and adds a constant offset to the variance. It originates from the readout noise of the camera and intensity-varying stray light. The second noise source is the atom shot noise, which describes the random variations due to the counting of atoms loaded until a given image index in the time trace. Its variance is equal to the average atom number. The recorded camera signal is directly proportional to the atom number $N_c = C N_{at}$, leading through error propagation to a variance of $C \bar{N}_c$. The two independent noise sources add up in their variances

$$\Delta_c^2 = C \bar{N}_c + \Delta_{bg}^2. \quad (1)$$

This theoretical prediction agrees well with the experimental observations (see supplementary information for further details). The calibration constant $C_{Na} = 1.15(5) \times 10^4$ and the background noise $\Delta_{bg,Na} = 2201(2)$ were independently extracted from a histogram plot, as described in "Full counting statistics of sodium" section. This validates our assumption that background and shot noise are the dominating noise sources for sodium. Converting the camera counts back into atom numbers, we obtain a resolution of 0.20(1) atoms, quantifying the quality of the observed single atom resolution. The connection of this resolution to the detection fidelity can be directly extracted from the histogram, shown in Fig. 6.

For potassium, we observe a more complex behavior of the variance. In the regime of few counts the variance is again dominated by the background noise and the atom shot noise. With the noise model (1), validated for sodium, we perform a fit to extract the calibration factor $C_K = 560(140)$ and the background noise $\Delta_{bg,K} = 2450(140)$. The resulting atom resolution of 4.3(1.1) atoms is similar to that achieved in precision experiments with Bose–Einstein condensates^{17,56}.

For higher atom numbers, we observe a non-linear dependence, which we attribute to technical fluctuations of the MOT. The MOT properties can be parameterized by the loading rate Γ_{load} and loss rate Γ_{loss} . Considering single atom load and loss only, they are connected to the atom number dynamics through

$$N_{at}(t) = \frac{\Gamma_{load}}{\Gamma_{loss}} [1 - \exp(-\Gamma_{loss}t)]. \quad (2)$$

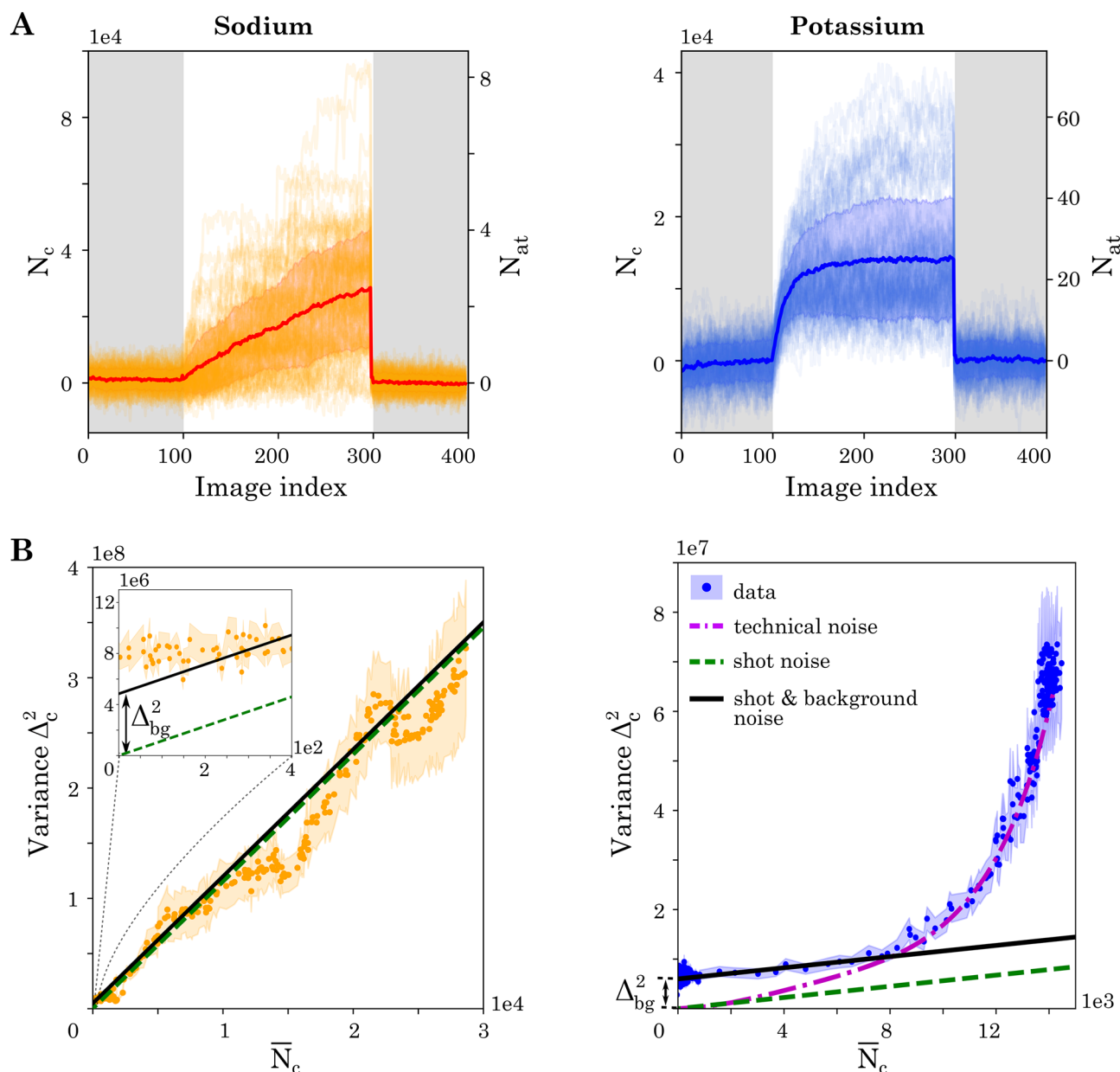


Figure 5. Characterization of atom number fluctuations for sodium (left) and potassium (right). **A:** Hundred time traces of sodium and potassium with mean and error band (shown as thick lines with shaded region around them). The figures show time traces both in units of camera counts (N_c) and atom number (N_{at}). **B:** Dependence of variance on mean camera counts. For sodium (left) the inset shows the background noise level.

We fit each time trace with this solution and, hence, extract the distribution of Γ_{load} and Γ_{loss} across different runs. The variance in the atom number dynamics, resulting from these fluctuations, is traced as the dash-dotted curve in Fig. 5B. In the high atom number regime it agrees well with our experimental observation. We expect to substantially reduce these fluctuations in the future by improving the stability of intensity, frequency, and magnetic field.

Full counting statistics of sodium

Going one step beyond the statistical analysis of ensemble averages, we use the single atom resolution of sodium to extract its full counting statistics^{57,58}. This requires the digitization of camera counts into discrete atom numbers³¹, as presented in Fig. 6. For this, we aggregate the camera counts of 100 runs into one histogram, which shows distinct atom number peaks. The calibration from camera counts to atom counts is accomplished through Gaussian fits to individual single atom peaks. The distance between consecutive peaks corresponds to the calibration factor $C_{Na} = 1.15(5) \times 10^4$. The width of the zero atom signal sets the background noise limit $\Delta_{bg,Na} = 2201(2)$ (these values are used in "Atom number dynamics" section in the analysis of the variance as a function of the mean camera counts \bar{N}_c). From the overlap of the peaks, we estimate the detection fidelity of

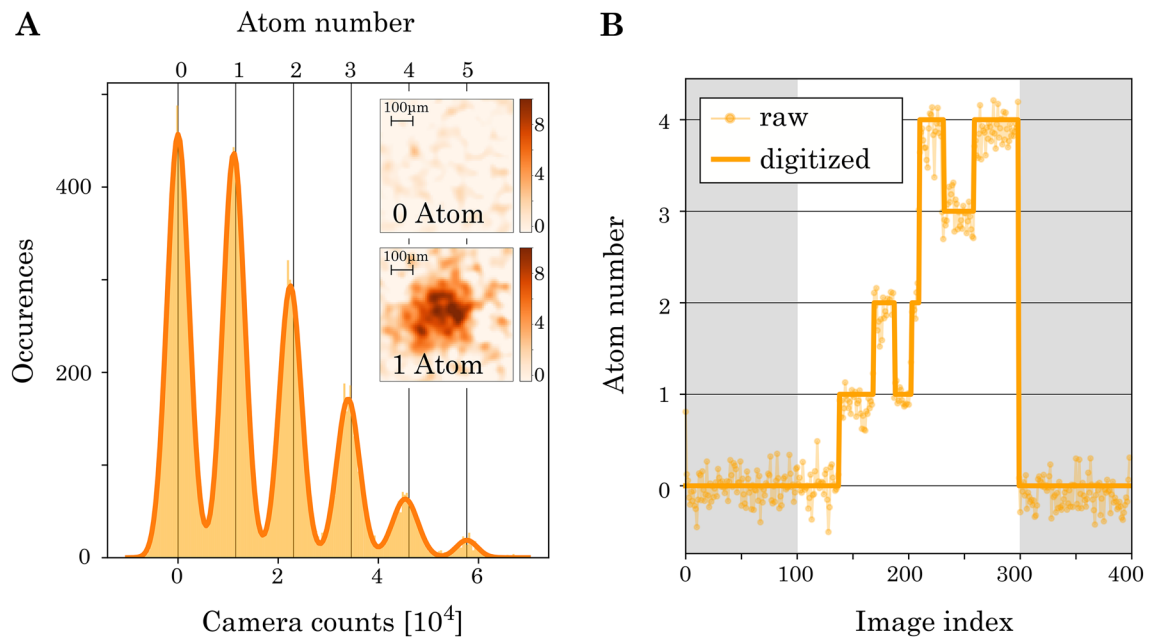


Figure 6. Accurate atom counting of sodium. **A:** Histogram of recorded camera counts. The calibration from camera counts to atom number is accomplished through Gaussian fits to distinct single atom peaks. Insets show average images of zero and one atom. **B:** Example time trace before and after digitization.

atoms to 96(3)%. With this calibration, we convert the time traces of camera counts into digitized atom number dynamics, as shown in Fig. 6B.

Each change in atom counts corresponds to a load or loss event with one or more atoms, as shown in Fig. 7A. We observe that the dynamics are dominated by single atom events, as only 3% involve two or more atoms. Therefore, we neglect them in the following. We count the number of single atom events in each time trace and summarize them in a histogram, shown in Fig. 7B.

On average we observe $\bar{N}_{\text{load}} = 2.02(6)$ loading events per time trace, which is much smaller than the total number of images $N_{\text{img}} = 200$ taken per time trace. Given that the atoms come from a large reservoir, namely the oven region, the loading rate is independent of the number of loaded atoms. From these observations, we describe the loading process statistically as a series of independent Bernoulli trials with a success probability p_{load} . Therefore, the single atom loading probability is given by

$$p_{\text{load}} = \frac{\bar{N}_{\text{load}}}{N_{\text{img}}}. \quad (3)$$

The large number of images and the low loading probability means that the number of loading events N_{load} converges towards a Poisson distribution with mean \bar{N}_{load} . This stands in full agreement with the experimental observation.

Once an atom is present, it can be lost from the MOT with a probability p_{loss} . We observe an average number of $\bar{N}_{\text{loss}} = 1.29(5)$ loss events per time trace. Since we do not distinguish between atoms, the number of atoms lost in each time step can be described by a binomial distribution. Therefore, the average number of single atom loss events per time trace \bar{N}_{loss} enables us to extract the loss probability

$$p_{\text{loss}} = \frac{\bar{N}_{\text{loss}}}{\sum_i \bar{N}_i}. \quad (4)$$

The normalization factor is the sum of average number of atoms present in each image i . Similar to the loading case, we observe a Poisson distribution for the loss events with mean \bar{N}_{loss} , which can be attributed to the occurrence of only a few loss events over a large set of images.

To study the influence of the large potassium cloud on the dynamics of the few sodium atoms, we compare the load and loss statistics of the sodium atom counts with and without potassium atoms present (see Fig. 7B). The extracted load and loss probabilities are summarized in Table 1. The values corresponding to the absence and presence of potassium are indistinguishable to roughly within five percent. To exclude experimental errors, we repeated the analysis for various configurations of relative positions of the two clouds, magnetic field gradients and laser detunings. All results were compatible with our observation of no influence of potassium on the sodium atom dynamics. We attribute these results to the extremely low density of the atomic clouds. To increase the density of both clouds in future studies, we plan to work at higher magnetic field gradients with water-cooled coils⁵⁹. At higher densities, we expect to observe inter-species interaction, which should influence the loading dynamics similar to previous studies^{26,40}.

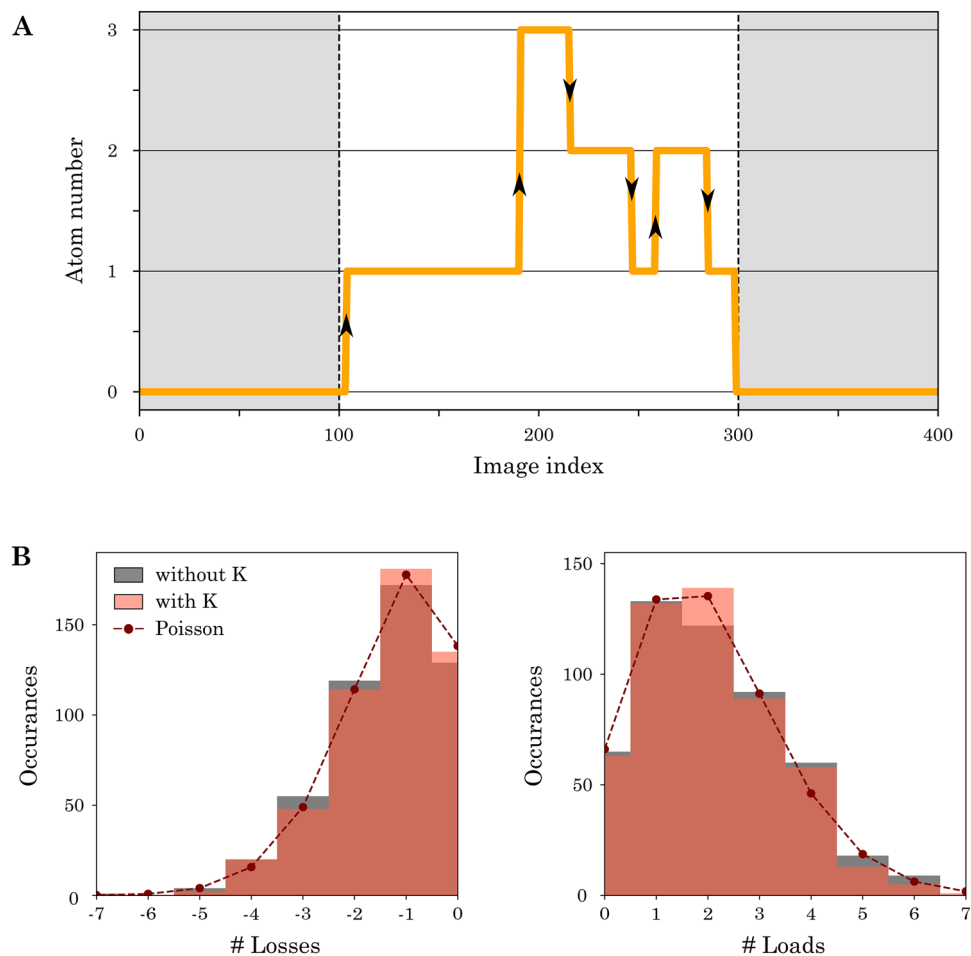


Figure 7. Counting statistics of sodium with and without potassium atoms present. **A:** Digitized example time trace of sodium with single atom load (loss) events marked with up (down) arrows. Only jumps during the MOT loading stage are taken into account. **B:** Histogram of the number of single atom losses and loads per time trace. The dashed lines show Poisson distributions with mean \bar{N}_{loss} and \bar{N}_{load} (extracted from the counting statistics).

	p_{load} [%]	p_{loss} [%]
Without K	1.06(3)	2.76(23)
With K	1.02(3)	2.47(24)

Table 1. Comparison of load and loss probabilities in a few atom sodium MOT with and without the presence of a potassium cloud. The uncertainties were obtained through bootstrap resampling.

Outlook

In this work, we presented a detailed experimental study of the stochastic dynamics of a few cold ^{23}Na atoms in presence of a cloud of ^{39}K atoms in a MOT. At low atomic densities present in the experiment, we found no influence of the potassium atoms on the sodium atom dynamics. Increasing the density should allow us to explore the inter-species interaction^{26,40}.

The experimental setup is designed to be directly extendable towards quantum degenerate gases through evaporative cooling⁴⁶. Defect-free optical tweezer arrays will provide high control over single atoms^{38,39} and their repeated observation, as recently demonstrated for strontium atoms⁶⁰. Such repeated measurements are necessary for the realization of quantum error correction schemes, where the logical qubits are implemented in the optical tweezers and the Bose–Einstein condensate mediates entanglement between them⁶¹.

Our study opens the path for investigating time-resolved dynamics, including transport and thermalization, in atomic mixtures over a wide range of parameters. The emergence of ergodicity will become directly observable as the equivalence of the ensemble averages with time averages for individual time traces for sufficiently long

times. Optimizing the photon detection should further allow us to reduce imaging times sufficiently to reach position-resolution^{29,30} without a pinning lattice²⁷. This will extend our work towards the quantum regime, in which we might continuously monitor thermalization of impurity atoms in a Bose-Einstein condensate^{35,62}.

The data that support the findings of this study are openly available at the following URL/DOI: <https://doi.org/10.11588/data/HRCX1P>.

Received: 22 September 2021; Accepted: 14 January 2022

Published online: 14 February 2022

References

- Cont, R. & Bouchaud, J.-P. Herd behavior and aggregate fluctuations in financial markets. *Macroecon. Dyn.* **4**, 170–196. <https://doi.org/10.1017/S1365100500015029> (2000).
- Kucsko, G. *et al.* Nanometre-scale thermometry in a living cell. *Nature* **500**, 54–58 (2013).
- Grusdt, F. & Demler, E. New theoretical approaches to Bose polarons. In *Quantum Matter at Ultralow Temperatures* **325**. <https://doi.org/10.3254/978-1-61499-694-1-325> (2016).
- Gluzza, M. *et al.* Quantum Field Thermal Machines. *PRX Quantum* **2**, 030310 (2021).
- Gröblacher, S., Hammerer, K., Vanner, M. R. & Aspelmeyer, M. Observation of strong coupling between a micromechanical resonator and an optical cavity field. *Nature* **460**, 724–727 (2009).
- Gleyzes, S. *et al.* Quantum jumps of light recording the birth and death of a photon in a cavity. *Nature* **446**, 297–300 (2007).
- Saira, O.-P. *et al.* Test of the Jarzynski and Crooks fluctuation relations in an electronic system. *Phys. Rev. Lett.* **109**, 180601. <https://doi.org/10.1103/PhysRevLett.109.180601> (2012).
- Maier, C. *et al.* Environment-assisted quantum transport in a 10-qubit network. *Phys. Rev. Lett.* **122**, 050501. <https://doi.org/10.1103/PhysRevLett.122.050501> (2019).
- Chiu, C. S. *et al.* String patterns in the doped hubbard model. *Science* **365**, 251–256. <https://doi.org/10.1126/science.aav3587> (2019).
- Banaszek, K., Cramer, M. & Gross, D. Focus on quantum tomography. *New J. Phys.* **15**, 125020. <https://doi.org/10.1088/1367-2630/15/12/125020> (2013).
- Steffen, M. *et al.* Measurement of the entanglement of two superconducting qubits via state tomography. *Science* **313**, 1423–1425. <https://doi.org/10.1126/science.1130886> (2006).
- Elben, A., Vermersch, B., Dalmonte, M., Cirac, J. I. & Zoller, P. Rényi entropies from random quenches in atomic hubbard and spin models. *Phys. Rev. Lett.* **120**, 050406. <https://doi.org/10.1103/PhysRevLett.120.050406> (2018).
- Brydges, T. *et al.* Probing rényi entanglement entropy via randomized measurements. *Science* **364**, 260–263. <https://doi.org/10.1126/science.aau4963> (2019).
- Gärtner, M. *et al.* Measuring out-of-time-order correlations and multiple quantum spectra in a trapped-ion quantum magnet. *Nat. Phys.* **13**, 781–786. <https://doi.org/10.1038/nphys4119> (2017).
- Schweigler, T. *et al.* Experimental characterization of a quantum many-body system via higher-order correlations. *Nature* **545**, 323–326. <https://doi.org/10.1038/nature22310> (2017).
- Avenhaus, M., Laiho, K., Chekhova, M. V. & Silberhorn, C. Accessing higher order correlations in quantum optical states by time multiplexing. *Phys. Rev. Lett.* **104**, 063602. <https://doi.org/10.1103/PhysRevLett.104.063602> (2010).
- Strobel, H. *et al.* Fisher information and entanglement of non-Gaussian spin states. *Science* **345**, 424–427. <https://doi.org/10.1126/science.1250147> (2014).
- Lukin, A. *et al.* Probing entanglement in a many-body-localized system. *Science* **364**, 256. <https://doi.org/10.1126/science.aau0818> (2019).
- Scelle, R., Rentrop, T., Trautmann, A., Schuster, T. & Oberthaler, M. K. Motional Coherence of Fermions Immersed in a Bose Gas. *Phys. Rev. Lett.* **111**, 070401. <https://doi.org/10.1103/PhysRevLett.111.070401> (2013).
- Rentrop, T. *et al.* Observation of the phononic Lamb shift with a synthetic vacuum. *Phys. Rev. X* **6**, 041041. <https://doi.org/10.1103/PhysRevX.6.041041> (2016).
- Jørgensen, N. B. *et al.* Observation of attractive and repulsive polarons in a Bose–Einstein condensate. *Phys. Rev. Lett.* **117**, 055302. <https://doi.org/10.1103/PhysRevLett.117.055302> (2016).
- Yan, Z. Z., Ni, Y., Robens, C. & Zwerlein, M. W. Bose polarons near quantum criticality. *Science* **368**, 190–194. <https://doi.org/10.1126/science.aax5850> (2020).
- Zohar, E., Cirac, J. I. & Reznik, B. Quantum simulations of lattice gauge theories using ultracold atoms in optical lattices. *Rep. Progress Phys.* **79**, 014401 (2015).
- Kasper, V., Hebenstreit, F., Jendrzejewski, F., Oberthaler, M. K. & Berges, J. Implementing quantum electrodynamics with ultracold atomic systems. *New J. Phys.* **19**, 023030. <https://doi.org/10.1088/1367-2630/aa54e0> (2017).
- Mil, A. *et al.* A scalable realization of local U(1) gauge invariance in cold atomic mixtures. *Science* **367**, 1128–1130. <https://doi.org/10.1126/science.aaz5312> (2020).
- Weber, C., John, S., Spethmann, N., Meschede, D. & Widera, A. Single Cs atoms as collisional probes in a large Rb magneto-optical trap. *Phys. Rev. A* **82**, 042722. <https://doi.org/10.1103/PhysRevA.82.042722> (2010).
- Hohmann, M. *et al.* Individual Tracer Atoms in an Ultracold Dilute Gas. *Phys. Rev. Lett.* **118**, 1–5. <https://doi.org/10.1103/PhysRevLett.118.263401> (2017).
- Bouton, Q. *et al.* Single-atom quantum probes for ultracold gases boosted by nonequilibrium spin dynamics. *Phys. Rev. X* **10**, 11018. <https://doi.org/10.1103/PhysRevX.10.11018> (2020).
- Bergschneider, A. *et al.* Spin-resolved single-atom imaging of Li 6 in free space. *Phys. Rev. A* **97**, 063613. <https://doi.org/10.1103/PhysRevA.97.063613> (2018).
- Bergschneider, A. *et al.* Experimental characterization of two-particle entanglement through position and momentum correlations. *Nat. Phys.* **15**, 640. <https://doi.org/10.1038/s41567-019-0508-6> (2019).
- Choi, Y. *et al.* Direct measurement of loading and loss rates in a magneto-optical trap with atom-number feedback. *Phys. Rev. A* **76**, 013402. <https://doi.org/10.1103/PhysRevA.76.013402> (2007).
- Ueberholz, B., Kuhr, S., Frese, D., Gomer, V. & Meschede, D. Cold collisions in a high-gradient magneto-optical trap. *J. Phys. B Atom. Molecul. Opt. Phys.* **35**, 4899–4914 (2002).
- Wenz, A. N. *et al.* From Few to Many: Observing the Formation of a Fermi Sea One Atom at a Time. *Science* **342**, 457–460. <https://doi.org/10.1126/science.1240516> (2013).
- Hume, D. B. *et al.* Accurate atom counting in mesoscopic ensembles. *Phys. Rev. Lett.* **111**, 253001. <https://doi.org/10.1103/PhysRevLett.111.253001> (2013).
- Hohmann, M. *et al.* Single-atom thermometer for ultracold gases. *Phys. Rev. A* **93**, 043607. <https://doi.org/10.1103/PhysRevA.93.043607> (2016).

36. Schmidt, F. *et al.* Precision measurement of the Rb 87 tune-out wavelength in the hyperfine ground state $F=1$ at 790 nm. *Phys. Rev. A* **93**, 022507. <https://doi.org/10.1103/PhysRevA.93.022507> (2016).
37. Schulze, T. *et al.* Feshbach spectroscopy and dual-species Bose–Einstein condensation of ^{23}Na – ^{39}K mixtures. *Phys. Rev. A* **97**, 023623. <https://doi.org/10.1103/physreva.97.023623> (2018).
38. Barredo, D., de Léséleuc, S., Lienhard, V., Lahaye, T. & Browaeys, A. An atom-by-atom assembler of defect-free arbitrary two-dimensional atomic arrays. *Science* **354**, 1021–1023 <https://doi.org/10.1126/science.aah3778> (2016).
39. Endres, M. *et al.* Atom-by-atom assembly of defect-free one-dimensional cold atom arrays. *Science* **354**, 1024–1027 <https://doi.org/10.1126/science.aah3752> (2016).
40. Castilho, P. C. M. *et al.* A compact experimental machine for studying tunable Bose–Bose superfluid mixtures. *Laser Phys. Lett.* **16**, 035501 (2019).
41. Kraft, S. *et al.* Formation of ultracold LiCs molecules. *J. Phys. B Atom. Mol. Opt. Phys.* **39**, S993. <https://doi.org/10.1088/0953-4075/39/19/S13> (2006).
42. Kemp, S. L. *et al.* Production and characterization of a dual species magneto–optical trap of cesium and ytterbium. *Rev. Sci. Instrum.* **87**, 023105. <https://doi.org/10.1063/1.4941719> (2016).
43. Martí, G., Olf, R., Vogt, E., Öttl, A. & Stamper-Kurn, D. Two-element Zeeman slower for rubidium and lithium. *Phys. Rev. A* **81**, 043424. <https://doi.org/10.1103/PhysRevA.81.043424> (2010).
44. Stan, C. A. & Ketterle, W. Multiple species atom source for laser-cooling experiments. *Rev. Sci. Instrum.* **76**, 6–11 <https://doi.org/10.1063/1.1935433> (2005).
45. Tiecke, T. G., Gensemer, S. D., Ludewig, A. & Walraven, J. T. M. High-flux two-dimensional magneto–optical-trap source for cold lithium atoms. *Phys. Rev. A* **80**, 013409. <https://doi.org/10.1103/PhysRevA.80.013409> (2009).
46. Lamporesi, G., Donadello, S., Serafini, S. & Ferrari, G. Compact high-flux source of cold sodium atoms. *Rev. Sci. Instrum.* **84**, 063102. <https://doi.org/10.1063/1.4808375> (2013).
47. Weis, A. & Derler, S. Doppler modulation and Zeeman modulation: Laser frequency stabilization without direct frequency modulation. *Appl. Opt.* **27**, 2662. <https://doi.org/10.1364/ao.27.002662> (1988).
48. Neuhaus, L. *et al.* Pyrp1 (python red pitaya lockbox) - an open-source software package for fpga-controlled quantum optics experiments. In *2017 Conference on Lasers and Electro-Optics Europe European Quantum Electronics Conference (CLEO/Europe-EQEC)*, 1–1, <https://doi.org/10.1109/CLEO-EQEC.2017.8087380> (2017).
49. Lamporesi, G., Donadello, S., Serafini, S., Dalfó, F. & Ferrari, G. Spontaneous creation of Kibble–Zurek solitons in a Bose–Einstein condensate. *Nat. Phys.* **9**, 656–660 (2013).
50. Farolfi, A. *et al.* Manipulation of an elongated internal Josephson junction of bosonic atoms. *Phys. Rev. A* **104**, 023326 (2021).
51. Picken, C. J., Legaie, R. & Pritchard, J. D. Single atom imaging with an sCMOS camera. *Appl. Phys. Lett.* **111**, 164102. <https://doi.org/10.1063/1.5003304> (2017).
52. Schlederer, M., Mozdzen, A., Lompe, T. & Moritz, H. Single atom counting in a two-color magneto-optical trap. *Phys. Rev. A* **103**, 033308 (2021).
53. Starkey, P. *et al.* A scripted control system for autonomous hardware-timed experiments. *Rev. Sci. Instrum.* **84**, 085111. <https://doi.org/10.1063/1.4817213> (2013).
54. Muessel, W. *et al.* Optimized absorption imaging of mesoscopic atomic clouds. *Appl. Phys. B* **113**, 69–73 (2013).
55. Kang, S., Yoon, S., Choi, Y., Lee, J.-H. & An, K. Dependence of fluorescence-level statistics on bin-time size in a few-atom magneto-optical trap. *Phys. Rev. A* **74**, 013409. <https://doi.org/10.1103/PhysRevA.74.013409> (2006).
56. Muessel, W., Strobel, H., Linnemann, D., Hume, D. & Oberthaler, M. Scalable Spin Squeezing for Quantum-Enhanced Magnetometry with Bose–Einstein Condensates. *Phys. Rev. Lett.* **113**, 103004. <https://doi.org/10.1103/PhysRevLett.113.103004> (2014).
57. Bouton, Q. *et al.* A quantum heat engine driven by atomic collisions. *Nat. Commun.* **12**, 2063. <https://doi.org/10.1038/s41467-021-22222-z> (2021).
58. Esposito, M., Harbola, U. & Mukamel, S. Nonequilibrium fluctuations, fluctuation theorems, and counting statistics in quantum systems. *Rev. Mod. Phys.* **81**, 1665–1702 <https://doi.org/10.1103/RevModPhys.81.1665> (2009).
59. Roux, K., Cilenti, B., Helson, V., Konishi, H. & Brantut, J.-P. Compact bulk-machined electromagnets for quantum gas experiments. *SciPost Phys.* **6**, 048. <https://doi.org/10.21468/SciPostPhys.6.4.048> (2019).
60. Covey, J. P., Madjarov, I. S., Cooper, A. & Endres, M. 2000-times repeated imaging of strontium atoms in clock-magic tweezer arrays. *Phys. Rev. Lett.* **122**, 173201. <https://doi.org/10.1103/PhysRevLett.122.173201> (2019).
61. Kasper, V. *et al.* Universal quantum computation and quantum error correction with ultracold atomic mixtures. *Quantum Sci. Technol.* **7**, 015008 (2022).
62. Mehboudi, M. *et al.* Using polarons for sub-nk quantum nondemolition thermometry in a bose-einstein condensate. *Phys. Rev. Lett.* **122**, 030403. <https://doi.org/10.1103/PhysRevLett.122.030403> (2019).

Acknowledgements

The authors are grateful for fruitful discussions and experimental help from Apoorva Hegde, Andy Xia, Alexander Hesse, Helmut Strobel, Valentin Kasper, Lisa Ringena and all the members of SynQS. We thank Giacomo Lamporesi as well as Gretchen K. Campbell and her team for valuable input on the design of the experimental setup. This work is part of and supported by the DFG Collaborative Research Centre “SFB 1225 (ISOQUANT)”. F. J. acknowledges the DFG support through the project FOR 2724, the Emmy- Noether Grant (Project-ID 377616843) and support by the Bundesministerium für Wirtschaft und Energie through the project “EnerQuant” (Project- ID 03EI1025C).

Author contributions

R.P.B., J.K. and L.H. set up the experiment and performed the measurements. F.J. supervised the project. All authors analysed the results. All authors reviewed the manuscript.

Funding

Open Access funding enabled and organized by Projekt DEAL. This work is part of and supported by the DFG Collaborative Research Centre “SFB 1225 (ISOQUANT)”. F. J. acknowledges the DFG support through the project FOR 2724, the Emmy- Noether Grant (Project-ID 377616843) and support by the Bundesministerium für Wirtschaft und Energie through the project “EnerQuant” (Project- ID 03EI1025C).

Competing interests

The authors declare no competing interests.

Additional information

Supplementary Information The online version contains supplementary material available at <https://doi.org/10.1038/s41598-022-05778-8>.

Correspondence and requests for materials should be addressed to R.P.B. or F.J.

Reprints and permissions information is available at www.nature.com/reprints.

Publisher's note Springer Nature remains neutral with regard to jurisdictional claims in published maps and institutional affiliations.



Open Access This article is licensed under a Creative Commons Attribution 4.0 International License, which permits use, sharing, adaptation, distribution and reproduction in any medium or format, as long as you give appropriate credit to the original author(s) and the source, provide a link to the Creative Commons licence, and indicate if changes were made. The images or other third party material in this article are included in the article's Creative Commons licence, unless indicated otherwise in a credit line to the material. If material is not included in the article's Creative Commons licence and your intended use is not permitted by statutory regulation or exceeds the permitted use, you will need to obtain permission directly from the copyright holder. To view a copy of this licence, visit <http://creativecommons.org/licenses/by/4.0/>.

© The Author(s) 2022